Analysis of Drell-Yan lepton pair production in the $p - p(\bar{p})$ colliders using different angular ordering constraints and the k_t-factorization approach

M. Modarres,[*] R. Taghavi, R. Aminzadeh Nik, and R. Kord Valeshabadi
Department of Physics, University of Tehran, 1439955961 Tehran, Iran

In this work, the $p - p(\bar{p})$ Drell-Yan lepton pair production (DY) differential cross sections at hadron colliders, such as LHC and TEVATRON, are studied in the k_t-factorization framework. In order to take into account the transverse momenta of incoming partons, we use the unintegrated parton distribution functions of Kimber *et al.* (KMR) and Martin *et al.* (MRW) in the leading order (LO), and next-to-leading-order (NLO) levels with the input MMHT2014 PDF libraries. Based on the different off shell partonic matrix elements, we analyze the behaviors of DY differential cross sections with respect to the invariant mass, the transverse momentum and the rapidity as well as the specific angular correlation between the produced leptons. The numerical results are compared with the experimental data, in different energies, which are reported by various collaborations, such as CDF, CMS, ATLAS, and LHCb. It is shown that the NLO-MRW and KMR schemes predict closer results to the data compared to the LO-MRW, since we do not have fragmentation. It is demonstrated that while the $q^* + \bar{q}^* \rightarrow \gamma^*/Z + g \rightarrow l^+ + l^- + g$ subprocess has a negligible contribution, it has a sizable effect in the low dilepton transverse momentum. In agreement with the NNLO, perturbative quantum chromodynamics (pQCD), report (PYTHIA, SHERPA, etc.) by including the higher-order perturbative contributions the better results are archived. On the other hand as the scale of energy increases, for the LHC energies, the Compton subprocess, i.e., $q^* + g^* \rightarrow \gamma^*/Z \rightarrow l^+ + l^- + q$, has the largest contribution to the differential cross section in the most intervals of some observables, as is expected. The variation of the differential cross section with respect to the various variables such as the invariant mass, the center of mass energy, etc. are discussed. In order to validate our results, we also consider the strong ordering constraint and the KaTie parton-level event generator.

I. INTRODUCTION

Traditionally, the Dokshitzer-Gribov-Lipatov-Altarelli-Parisi (DGLAP) evolution equations [1–4] approach is used to obtain the quark, antiquark and gluon densities, i.e., the parton distribution functions (PDF), $a(x, \mu^2)$. These functions depend on the Bjorken variable x and the hard scale μ^2, and can be easily used in the collinear QCD factorization formalisms. In these DGLAP evolution approaches, the transverse momentum (k_t) components of partons are integrated over and there is not any degree of freedom for the initial gluon radiations and the transverse momentum (k_t) of the partons in the PDF. The outcome of hadron-hadron colliders at high energies indicates that the explicit inclusion of the intrinsic transverse momentum of initial hadron constituents is important to get accurate results and

predictions. Therefore, the important inputs are the transverse momentum dependent parton distribution functions or the so-called "unintegrated" PDF (UPDF).

Theoretically, various methods are proposed to generate these fundamental quantities, i.e., UPDF, and among them the Balitsky-Fadin-Kuraev-Lipatov [5–9] (which is valid for the small x and the scale k_t^2) and Catani-Ciafaloni-Fiorani-Marchesini (CCFM) [10–14] (which is applicable at both the small and large x, the scales k_t^2 and μ^2) evolution equations are considered extensively. Nevertheless, the CCFM approach is both mathematically and numerically more complicated and time consuming.

Recently, Kimber *et al.* (KMR) [15] and Martin *et al.* (MRW) [16] proposed the KMR and MRW formalisms, respectively, in the leading order (LO) and next-to-leading order (NLO) levels. These formalisms were extensively used to extract the UPDF, $f(x, k_t^2, \mu^2)$, from the ordinary PDF based on the k_t-factorization approach of pQCD as well as probing the partonic structures of hadrons [17–21]. The main difference between these two approaches is originated from into the various types of imposing the angular ordering constraints (AOC). We analyzed these formalisms to calculate the proton structure functions and

the different hadron-hadron differential cross sections in the references [22–26].

The analysis of Drell-Yan lepton pair production (DY) in the hadron-hadron collisions at high energies is the subject of intense studies [27–35], since it provides an ideal ground for testing the QCD predictions [36–39]. Many experimental groups like the CDF, CMS, ATLAS, D0 and LHCb Collaborations [27–34] try to compare the experimental measurements of these DY (using the available energies of the Tevatron and LHC colliders events of the corresponding theoretical predictions from the pQCD and the parton level Monte Carlo programs, such as ResBos [40], DYNNLO [41], and POWHEG + PYTHIA [42] event generators. The ResBos method simulates the vector-boson production and its decay, using a resumed treatment of the soft-gluon emissions at the NLO-logarithm and the γ^* and Z/γ^* contributions are simulated at the NLO accuracies. The DYNNLO approach is a parton level Monte Carlo program that computes the cross sections for the vector boson production in the $p - p(\bar{p})$ collisions up to the NNLO in the pQCD theory. The PYTHIA program generates the LO QCD interactions via its parton shower algorithms. In a recent investigation [33] the distribution of dilepton transverse momentum and angular variable ϕ_η^* were calculated perturbatively at $\sqrt{s} = 8$ TeV using the ResBos Monte Carlo generator at NNLO accuracy and compared to the ATLAS data. Although, the results at low values of p_T and ϕ_η^* demonstrate good agreement with the data, this is not the case at high values of p_T and ϕ_η^*.

In the present report, it is intended to calculate the DY differential cross sections based on the KMR and MRW k_t-factorization approaches using the corresponding off shell transition amplitudes. We consider the three subprocesses namely; (1) $q^* + \bar{q}^* \to \gamma^*/Z \to l^+ + l^-$, (2) $q^* + g^* \to \gamma^*/Z \to l^+ + l^- + q$ and (3) $q^* + \bar{q}^* \to \gamma^*/Z + g \to l^+ + l^- + g$ at the LO and NLO levels, respectively. The dependence of the DY differential cross sections on the dilepton transverse momentum, the invariant mass and the rapidity distributions as well as the angular correlation between the produced leptons are calculated in the above frameworks and compared with the experimental data developed by the CDF, CMS, ATLAS and LHCb collaborations in both the Tevatron and LHC energies. The Harland-Lang *et al.* (MMHT2014) PDF libraries [43] in the LO for both the KMR [15] and MRW [16] formalisms and the NLO for NLO-MRW approaches are considered. These calculations are performed for the off shell incoming partons.

We should also point out here that, recently, the consideration of various angular ordering, as well as the generation of different UPDF becomes the subject of several reports [44,45]. In the reference [44], it is pointed out that the KMR UPDF, which are generated using the differential and integral approaches, give different results in the region where $k_t > \mu$. Therefore it is concluded that, the integral form of the KMR UPDF gives the correct result,

while for the application of differential form, one should use the cutoff dependent PDF. On the other hand, in the reference [46], the above idea is rejected, and a new term is added to the Sudakov form factor via a Heaviside step function, to set the Sudakov form factor equal to 1 in the region where $k_t > \mu$. Further, it is claimed that the above two forms of the KMR approach give the same result i.e., there is no need to introduce cutoff dependent PDF. Finally, in the reference [46], by referring to this report, i.e., [47] (in which the predictions of the KMR approach with the AOC overestimates the data in case of the heavy quark production) it is suggested that the above problem is due to the freedom of the parton to have transverse momentum larger than μ, and concluded that it is much more suitable to use the KMR UPDF with the strong ordering constraint (SOC), which harshly cuts the transverse momentum in $k_t > \mu$ region. Because of the above statements, and all of the problems appear in $k_t > \mu$, we compute the DY differential cross sections with respect to M^{ll} and p_T^{ll} using the SOC KMR UPDF to check the sensitivity of our results in this region [see Figs. 1 (panel f) and 2 (panel d)]. One should also note that, as is discussed in the reference [48], the result of k_t-factorization should not be as good as collinear factorization approaches in covering the experimental data—on the other hand, it is more simplistic considering computer time consumption.

It should be also noted that the Sudakov form factor of the KMR approach does not obey the multiplication law according to the reference [52], but despite of this fact, it is interesting to point out that the normalization condition [see Eq. (1)] is approximately satisfied in the KMR formalism (which is a critical issue in constructing any new UPDF).

The k_t-factorization calculations were also performed by considering one or two of the above three subprocesses with the MSTW2008 PDF [53–55]. In these works, although the authors declare that they use the KMR formalism, they do not take into account the factor $1/k_t^2$ in the cross section nor in the normalization formulas

$$xa(x,\mu^2) \simeq \int^{\mu^2} \frac{dk_t^2}{k_t^2} f(x, k_t^2, \mu^2). \qquad (1)$$

Additionally, they use different angular ordering conditions with respect to the KMR prescriptions (we refer to them as semi-KMR). However, their results are surprisingly close to the experimental data. In the above references [54,55], it is claimed that the second and the third of the above subprocesses can be omitted by effectively using only the reggeized (off shell) quark approach in the first subprocess. A brief discussion about the result of these reports and the comparison with our predictions are presented in the Sec. III. In reference [54], although the off shell initial quarks are used, it is shown that utilizing the reggeized model and the effective vertexes guarantee the gauge invariance of the transition matrix elements (TME). However, in our previous
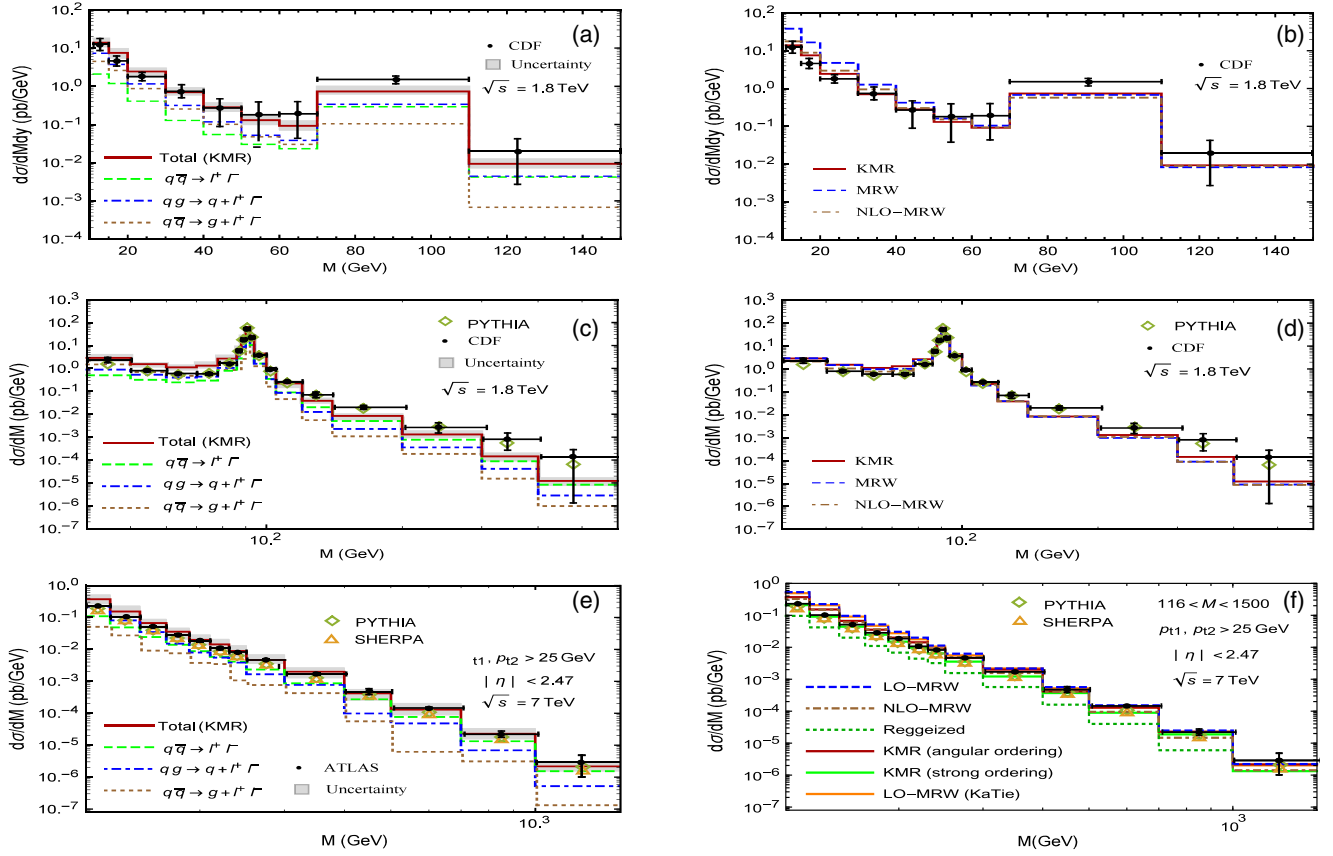
FIG. 1. The (double) differential cross sections of DY at Tevatron and LHC as a function of the dilepton invariant mass at $E_{CM} = 1.8$ and 7 TeV compared to the CDF and ATLAS data [49–51]. The numerical results related to the KMR UPDF are shown in left panels. The contribution of the $q^* + \bar{q}^* \to \gamma^*/Z \to l^+ + l^-$, $q^* + g^* \to \gamma^*/Z \to l^+ + l^- + q$ and $q^* + \bar{q}^* \to \gamma^*/Z + g \to l^+ + l^- + g$ sub-processes are presented by dash, dotted-dash and dotted histograms. In the right panels, the results corresponding to the KMR, LO and NLO-MRW UPDF are shown by solid, dashed and dotdashed histograms respectively and compared with each other. The shaded bands indicate the corresponding uncertainty for KMR calculations (see the text for details about the SOC and KaTie results).

work [56], we showed that using the off shell initial quarks in the k_t-factorization dynamics and in the small x regions leads to gauge invariance of the TME, too.

To check the validity of our calculated cross sections the KaTie parton-level event generator [57] is used (in which the off shell partonic cross sections are taken care of) and gives the hadronic cross section with desirable accuracy. However, we are not intending to solely show the result of cross section as it can be simply done with the KaTie parton-level event generator [57] [see Figs. 1 (panel f) and 2 (panel h)]. Our intention is to check the effects of different impositions of the cutoff Δ, which is additionally imposed on the quark radiation term in the KMR approach. We also want to check the other forms of the DGLAP based UPDF, i.e., NLO-MRW, in which Martin *et al.* used the virtuality $k^2 = k_t^2/(1-z)$. The UPDF of this form are rarely investigated in the phenomenological applications of the k_t-factorization. We include the subprocess $q^* + \bar{q}^* \to \gamma^*/Z \to l^+ + l^- + g$ which usually is neglected e.g., [53]. In the others works, including those that are cited in our paper [53], the combinations of KMR and MRW

formalisms are used incorrectly and they forget about the importance of the normalization constraint [Eq. (1)] on the UPDF. This point is discussed in detail in Ref. [56]. One should note that the KMR prescription is a semi-NLO. Another important item is the fragmentation effect, which are not presented in the processes that are discussed in our paper. Because of that, as it is explained in the paper, the KMR and NLO-MRW procedures demonstrate better agreement to the experimental data.

The outline of our paper is as follows. In Sec. II, we briefly present the basic cross section formulas of k_t-factorization (II A) approach and the derivation of input UPDF (II B). In Sec. III we present numerical calculations (III A), results presentations (III B), and discussions (III B). Section IV expresses our conclusions.

II. THE THEORETICAL FRAMEWORK OF DY

A. The k_t-factorization cross section formulas

Our DY differential cross section calculations are based on the k_t-factorization in the KMR and MRW UPDF [15,16] approaches. Therefore, in this section, we describe
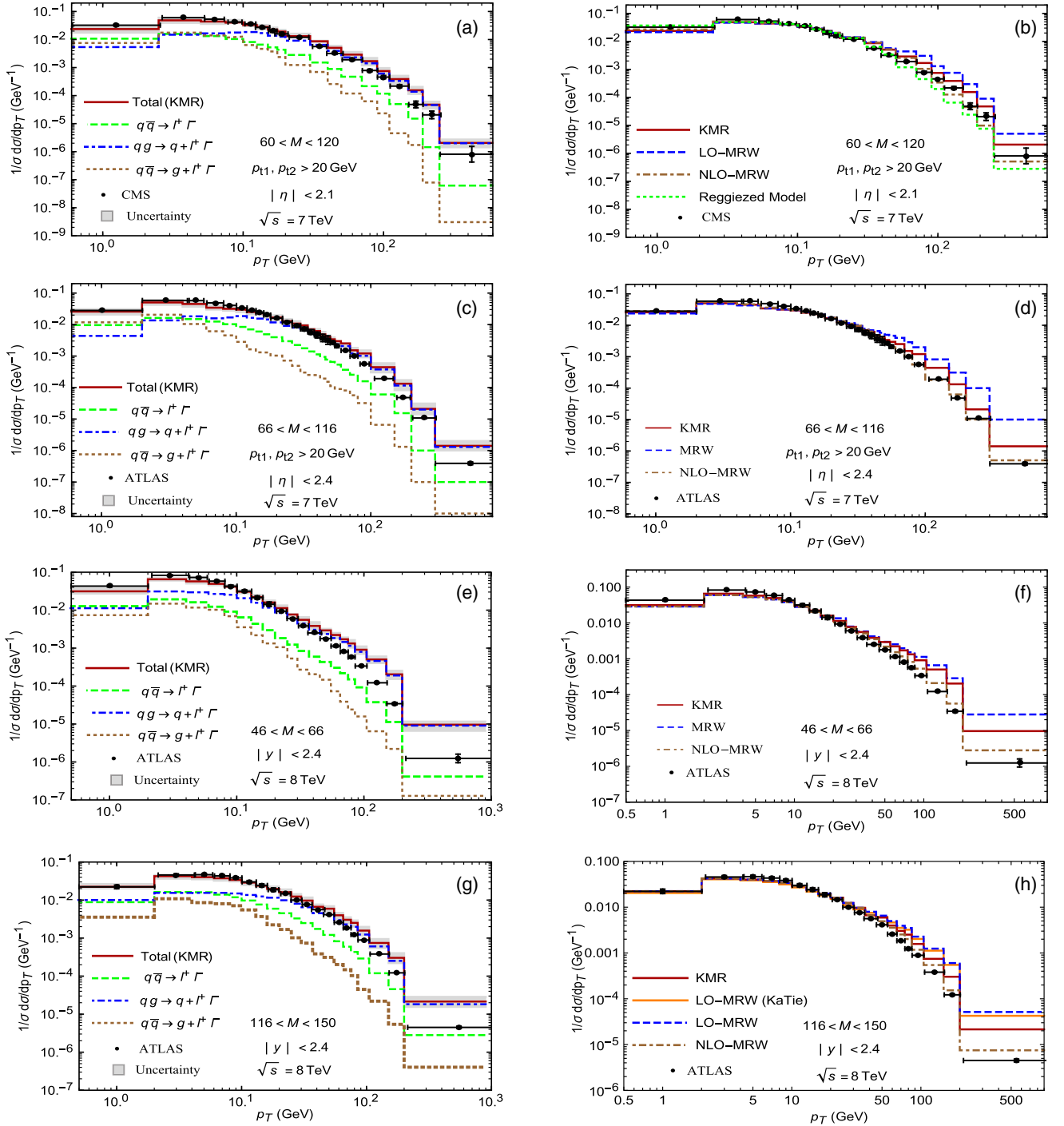
FIG. 2.   The normalized differential cross section of Drell-Yan lepton pair production at LHC as a function of the dilepton transverse momentum, at $E_{CM} = 7$ and 8 TeV compared to the different collaborations data from the CMS [27] and ATLAS [31,58]. The notation of all histograms is the same as in Fig. 1 (see the text for details about the SOC and KaTie results).

the theoretical framework of these approaches as well as the corresponding matrix elements (see Appendix A). As we pointed out in the introduction, we include all the subprocess contributions up to the $\alpha\alpha_s$ level, namely: $q^* + \bar{q}^* \rightarrow \gamma^*/Z \rightarrow l^+ + l^-$, $q^* + g^* \rightarrow \gamma^*/Z \rightarrow l^+ + l^- + q$ and $q^* + \bar{q}^* \rightarrow \gamma^*/Z + g \rightarrow l^+ + l^- + g$. From the kinematical point of view, if we show the four-momenta of

the incoming protons (partons) by $P^{(1)} (k^{(1)})$ and $P^{(2)} (k^{(2)})$ and neglect their masses, then in the proton center of mass framework we have

$$P^{(1)} = \frac{\sqrt{s}}{2} (1, 0, 0, 1), \qquad P^{(2)} = \frac{\sqrt{s}}{2} (1, 0, 0, -1), \qquad (2)$$

where $\sqrt{s}$ is the total center of mass energy. In the high energy and the leading log-approximation kinematics, the corresponding parton four-momenta can be written in terms of their transverse momenta k_{1t} and k_{2t}, and the fraction (x_i) of the incoming protons momentum as

$$k_1 = x_1 P^{(1)} + k_{1t}, \qquad k_2 = x_2 P^{(2)} + k_{2t}. \qquad (3)$$

There are some relations for the above three subprocesses due to the energy-momentum conservation law as follows:

$$k_{1t} + k_{2t} = p_{1t} + p_{2t}, \qquad (4)$$

$$x_1 = \frac{1}{\sqrt{s}}(m_{1t}e^{y_1} + m_{2t}e^{y_2}), \qquad (5)$$

$$x_2 = \frac{1}{\sqrt{s}}(m_{1t}e^{-y_1} + m_{2t}e^{-y_2}), \qquad (6)$$

for the first subprocess and

$$k_{1t} + k_{2t} = p_{1t} + p_{2t} + p_{3t}, \qquad (7)$$

$$x_1 = \frac{1}{\sqrt{s}}(m_{1t}e^{y_1} + m_{2t}e^{y_2} + m_{3t}e^{y_3}), \qquad (8)$$

$$x_2 = \frac{1}{\sqrt{s}}(m_{1t}e^{-y_1} + m_{2t}e^{-y_2} + m_{3t}e^{-y_3}). \qquad (9)$$

for the second and third subprocesses, where p_{it}, y_i and m_{it} are the transverse momenta, the rapidities and the transverse masses $(m_{it}^2 = m_i^2 + p_{it}^2)$ of the produced particles, [$i = 1$ and 2 for leptons, and $i = 3$ for (anti-) quark or gluon], respectively.

To calculate the matrix elements squared in the k_t-factorization framework [59], the summation over the incoming off shell gluon polarizations is carried out as

$$\sum \epsilon^\mu \epsilon^\nu = k_{2t}^\mu k_{2t}^\nu / k_{2t}^2, \qquad (10)$$

where k_t is the gluon transverse momentum. For the off shell quark spinors with momentum k (after imposing the Sudakov decomposition in the high energy and the leading log-approximation kinematics [60]), we have $\sum u(k)\bar{u}(k) \simeq \frac{x\hat{P}}{k_t^2}$, where x represents the fractional longitudinal momentum of the proton (see Refs. [56,61,62]). Also, the effective vertices are used to calculate the Feynman amplitudes to test and ensure the gauge invariance of the different matrix elements [63–65]. It is worth pointing out that a similar technique is also developed, using the Slavnov-Taylor identities by the means of the helicity amplitude [66–68] and being checked against those obtained by usage of Lipatovs effective action [63–65], as we pointed out.

To calculate the differential cross sections of DY, according to the k_t-factorization theorem, for $2 \to 2$ subprocess we have

$$\sigma_1 = \sum_q \int \frac{1}{16\pi(x_1 x_2 s)^2} |\mathcal{M}_1^{\gamma^*} + \mathcal{M}_1^Z|^2$$

$$\times f_q(x_1, k_{1t}^2, \mu^2) f_{\bar{q}}(x_2, k_{2t}^2, \mu^2) \frac{dk_{1t}^2}{k_{1t}^2}$$

$$\times \frac{dk_{2t}^2}{k_{2t}^2} dp_{1t}^2 dp_{2t}^2 dy_1 dy_2 \frac{d\phi_1}{2\pi} \frac{d\phi_2}{2\pi}, \qquad (11)$$

and for $2 \to 3$ subprocess one finds

$$\sigma_{2(3)} = \sum_q \int \frac{1}{256\pi^3(x_1 x_2 s)^2} |\mathcal{M}_{2(3)}^{\gamma^*} + \mathcal{M}_{2(3)}^Z|^2$$

$$\times f_q(x_1, k_{1t}^2, \mu^2) f_{g(\bar{q})}(x_2, k_{2t}^2, \mu^2) \frac{dk_{1t}^2}{k_{1t}^2}$$

$$\times \frac{dk_{2t}^2}{k_{2t}^2} dp_{1t}^2 dp_{2t}^2 dy_1 dy_2 dy_3 \frac{d\phi_1}{2\pi} \frac{d\phi_2}{2\pi} \frac{d\psi_1}{2\pi} \frac{d\psi_2}{2\pi}, \qquad (12)$$

where $f_q(x_i, k_{it}^2, \mu^2)$ are the UPDF, which depend on the two hard scales, k_t^2 and μ^2, and they can be written in terms of the usual PDF. As we pointed out in the Introduction, in the present calculations, the MMHT2014 PDF [43] is used for calculating the UPDF. In the above formula, $\mathcal{M}_i^j$ are the off shell matrix elements which are presented for the three different subprocesses in Appendix A. Note that when we square the matrix elements of each three subprocesses we get the interference effect between γ^* and Z production, which will be discussed in Sec. III. The azimuthal angles of the initial partons and the produced leptons are presented by ϕ_1 and ϕ_2, and ψ_1 and ψ_2, respectively. Then the total cross section can be written as

$$\sigma_{\text{Total}} = \sigma_1 + \sigma_2 + \sigma_3. \qquad (13)$$

To calculate the UPDF of (anti-)quarks and gluons in a proton, we apply the LO KMR, LO MRW and NLO-MRW approaches [15,16]. In the following each of them will be described.

B. The KMR and MRW UPDF

In the KMR method the UPDF of each parton (which means the probability to find a parton with transverse momentum k_t and fractional momentum x at hard scale μ^2) are given by

$$f_a(x, k_t^2, \mu^2) = T_a(k_t^2, \mu^2)$$
$$\times \sum_{b=q,g} \left[\frac{\alpha_S(k_t^2)}{2\pi} \int_x^{1-\Delta} dz P_{ab}^{(0)}(z) b\left(\frac{x}{z}, k_t^2\right) \right], \tag{14}$$

where $T_a(k_t^2, \mu^2)$ is

$$T_a(k_t^2, \mu^2) = \exp\left(- \int_{k_t^2}^{\mu^2} \frac{\alpha_S(k^2)}{2\pi} \frac{dk^2}{k^2} \right.$$
$$\left. \times \sum_{b=q,g} \int_0^{1-\Delta} dz' P_{ab}^{(0)}(z') \right), \tag{15}$$

which is the familiar Sudakov survival form factor and limits the emissions of partons between k_t^2 and μ^2 scales [15,16]. $P_{ab}^{(0)}(z)$ are the usual LO splitting functions. In this formula the angular-ordering constraint (AOC) [10–14,69,70], Δ, is applied in the upper limit of the integration, which is an infrared cutoff to prevent the soft gluon singularities arising from the splitting functions and is defined as

$$\Delta = \frac{k_t}{\mu + k_t}. \tag{16}$$

Note that this constraint is imposed on both quark and gluon radiations. $b(\frac{x}{z}, k_t^2)$ are the LO PDF, and in this work they are taken from the MMHT2014 libraries [43].

To determine the UPDF we also apply the MRW prescription which is similar to the KMR formalism, but the AOC only acts on the terms which include the on shell gluon emissions. For the quarks and the gluons they take the following forms:

$$f_q^{\text{LO}}(x, k_t^2, \mu^2)$$
$$= T_q(k_t^2, \mu^2) \frac{\alpha_S(k_t^2)}{2\pi} \int_x^1 dz \left[P_{qq}^{(0)}(z) \frac{x}{z} q\left(\frac{x}{z}, k_t^2\right) \right.$$
$$\left. \times \Theta\left(\frac{\mu}{\mu + k_t} - z\right) + P_{qg}^{(0)}(z) \frac{x}{z} g\left(\frac{x}{z}, k_t^2\right) \right], \tag{17}$$

with

$$T_q(k_t^2, \mu^2) = \exp\left(- \int_{k_t^2}^{\mu^2} \frac{\alpha_S(k^2)}{2\pi} \frac{dk^2}{k^2} \int_0^{z_{\max}} dz' P_{qq}^{(0)}(z') \right), \tag{18}$$

and

$$f_g^{\text{LO}}(x, k_t^2, \mu^2) = T_g(k_t^2, \mu^2) \frac{\alpha_S(k_t^2)}{2\pi} \int_x^1 dz \left[P_{gq}^{(0)}(z) \sum_q \frac{x}{z} q\left(\frac{x}{z}, k_t^2\right) + P_{gg}^{(0)}(z) \frac{x}{z} g\left(\frac{x}{z}, k_t^2\right) \Theta\left(\frac{\mu}{\mu + k_t} - z\right) \right], \tag{19}$$

with

$$T_g(k_t^2, \mu^2) = \exp\left(- \int_{k_t^2}^{\mu^2} \frac{\alpha_S(k^2)}{2\pi} \frac{dk^2}{k^2} \left[\int_{z_{\min}}^{z_{\max}} dz' z' P_{gg}^{(\text{LO})}(z') + n_f \int_0^1 dz' P_{qg}^{(0)}(z') \right] \right), \tag{20}$$

respectively. In the above equations, $z_{\max} = 1 - z_{\min} = \frac{\mu}{\mu+k_t}$ [71].

By expanding MRW to the NLO level, we have

$$f_a^{\text{NLO}}(x, k_t^2, \mu^2) = \int_x^1 dz T_a\left(k^2 = \frac{k_t^2}{(1-z)}, \mu^2\right) \frac{\alpha_S(k^2)}{2\pi} \sum_{b=q,g} \tilde{P}_{ab}^{(0+1)}(z) \times b^{\text{NLO}}\left(\frac{x}{z}, k^2\right) \Theta\left(1 - z - \frac{k_t^2}{\mu^2}\right). \tag{21}$$

In this formalism the Sudakov form factor is defined as

$$T_q(k^2, \mu^2) = \exp\left(- \int_{k^2}^{\mu^2} \frac{\alpha_S(q^2)}{2\pi} \frac{dq^2}{q^2} \int_0^1 dz' z' [\tilde{P}_{qq}^{(0+1)}(z') + \tilde{P}_{gq}^{(0+1)}(z')] \right), \tag{22}$$

$$T_g(k^2, \mu^2) = \exp\left(- \int_{k^2}^{\mu^2} \frac{\alpha_S(q^2)}{2\pi} \frac{dq^2}{q^2} \int_0^1 dz' z' [\tilde{P}_{gg}^{(0+1)}(z') + 2n_f \tilde{P}_{qg}^{(0+1)}(z')] \right). \tag{23}$$

The higher order splitting functions are presented in Appendix B.

III. NUMERICAL RESULTS AND DISCUSSIONS

A. Numerical calculations

In this section, we present the kinematics and theoretical inputs of our calculations. First, we calculate the UPDF based on the different k_t-factorization schemes by using two different methods, i.e., KMR and MRW. Through our calculations, we set the renormalization and factorization scales to be equal to $\mu_R = \mu_F = \zeta M$, in which $M = \sqrt{2p_{1t}p_{2t}[\cosh(y_1 - y_2) - \cos(\phi_1 - \phi_2)]}$ is the invariant mass of produced dileptons and as usual we consider the default value $\zeta = 1$ [56]. We let this parameter to vary from $1/2$ to 2, to estimate the scale uncertainties of our calculations. We also set $m_Z = 91.187$ GeV and $\Lambda_{\mathrm{QCD}} = 200$ MeV with $n_f = 4$ active quark flavors. Using the LO coupling constant, we get $\alpha_s(M_Z^2) = 0.123$ ($g_W = 0.66$). Second, with the massless quarks approximation, the calculation of transition matrix elements squared is carried out using the small x approximation presented in Appendix A, by the means of FeynCalc [72] i.e., the Mathematica package for symbolic semiautomatic evaluation of Feynman diagrams. In this paper, the nonlogarithmic loop corrections to the q-$\bar{q}$ annihilation cross section are taken into account by applying the effective K-factor with a particular scale choice of $\mu^2 = p_T^{4/3}M^{2/3}$ as it was done, for example, in the references [26,53,73], i.e.,

$$K = \exp\left[C_F \frac{\alpha_s(\mu^2)}{2\pi}\pi^2\right],$$

where p_T, $[p_T = |\vec{p}_{1t} + \vec{p}_{2t}|$, see above Eq. (9)] is the transverse momentum of produced dileptons and C_F is the color factor. To calculate the multidimensional integration, the VEGAS routine [74] is used. The differential cross sections at several center of mass energies, i.e., 1.96, 7, and 8 TeV as a function of the dilepton invariant mass (M), rapidity (y), transverse momentum (p_T), and the variable ϕ_η^* [34,75–77] i.e.,

$$\phi_\eta^* = \tan\left(\frac{\phi_{\mathrm{acop}}}{2}\right)\left[\cos\left(\frac{\Delta\eta}{2}\right)\right]^{-1},$$

are calculated with $\phi_{\mathrm{acop}} = \pi - |\Delta\phi|$, where $\Delta\eta$ and $\Delta\phi$ are the pseudorapidity and azimuthal angle differences between the produced leptons, respectively. The variable ϕ_η^* is correlated to the quantity $|p_T|/M$ and both of them probes the same physics as the dilepton transverse momentum, but it gives a better experimental resolution [78–80].

B. Results presentations

The results of above numerical calculations are compared with the experimental data of DY at the Tevatron and LHC laboratories with the total center of mass energy $\sqrt{s} = 1.8$ TeV and $\sqrt{s} = 7$ and 8 TeV, respectively. We use the data from different groups such as the CDF, CMS, ATLAS and LHCb collaborations. The available pQCD predictions are also presented in each figure.

The above comparisons are demonstrated in the Figs. 1–10 as follows:

(1) In all of the figures, the numerical results related to the KMR UPDF are shown in the left panels in which the dash, dotted-dash and dotted histograms correspond to the contribution of individual subprocesses, i.e., $q^* + \bar{q}^* \to \gamma^*/Z \to l^+ + l^-$, $q^* + g^* \to \gamma^*/Z \to l^+ + l^- + q$ and $q^* + \bar{q}^* \to \gamma^*/Z + g \to l^+ + l^- + g$ respectively. The shaded bands indicate the corresponding uncertainty ($\frac{1}{2} \leq \zeta \leq 2$) due to the hard scale variation with KMR UPDF in cross sections evaluation. Unlike the present paper, most of the previous phenomenological works with the semi-KMR UPDF for the DY differential cross sections did not present the contribution of each subprocess in their final results and also, did not take into account the contribution of the third subprocess (assuming the possible double counting [53,54] between the first and the third subprocesses). However, according to our previous papers [25,56], we do not believe that there is any double counting among the first and the third subprocesses. This point will be discussed in Sec. III C.

(2) In the right panels of each figure, the results of different UPDF applications, namely KMR, LO-MRW and NLO-MRW, in the differential cross sections are shown by the solid, dash and dotted-dash histograms, respectively, for the possible comparisons.

(3) Figs. 1–10, demonstrate the DY differential cross sections versus the dilepton invariant mass (M), the transverse momentum (p_T), the variable ϕ_η^* and the rapidity (y), respectively (see the caption of each figure for more details).

C. Discussions

First, we generally start by analyzing the calculated cross sections related to the medium and high center of mass energies for $\sqrt{s} = 1.8$ and 7 TeV. Although the results show that the KMR UPDF describe reasonably the wide range of data of Tevatron and LHC, we note that for the two sets of differential cross section data which are in terms of p_T and ϕ_η^* parameters, this is not the case. Indeed, in these two cases, the input NLO-MRW UPDF describe the data better than other schemes. To be sure about this conclusion, we try to include the newer data from the ATLAS Collaboration at $\sqrt{s} = 8$ TeV. The results of this double check are presented in the different panels of Figs. 2–8. The final comparisons (as we will discuss below) indicate that among the three different schemes (i.e., KMR, LO-MRW, and NLO-MRW UPDF) the NLO-MRW one, on average, is more suitable for describing the experimental data and it confirms other group reports of NNLO pQCD calculations [81]. We should point out here that in our previous work e.g., Ref. [56], the KMR and
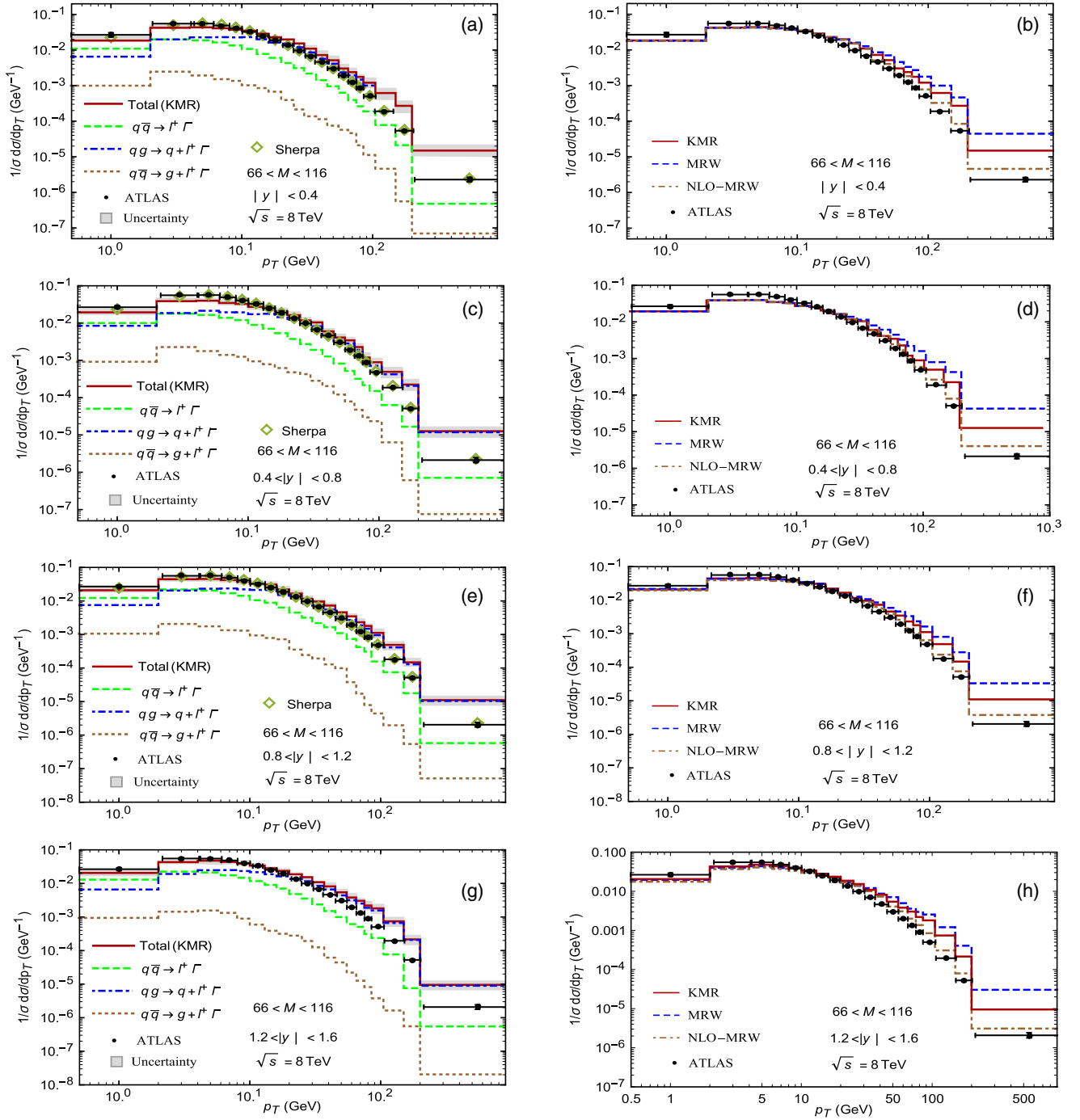
FIG. 3. The normalized differential cross section of Drell-Yan lepton pair production at LHC as a function of dilepton transverse momentum at $E_{CM} = 8$ TeV compared to the ATLAS data [33]. The notation of all histograms is the same as in Fig. 1.

LO-MRW had a better agreement to the data (because of the possible fragmentation effects).

The results of double and single differential cross sections $\frac{d\sigma}{dMdy}$ and $\frac{d\sigma}{dM}$ versus the invariant mass of the dilepton are compared to the experimental data at $\sqrt{s} = 1.8$ and 7 TeV and are shown in Fig. 1 (panels (a) and (b) and (c) to (f), respectively). In the panels (a) to (d) of this figure, as is expected, the Z boson mass peak is observed around

the $M = 91$ GeV. In these panels, it is clear that in the small M region ($M < M_z$) which corresponds to the medium and large p_T, the contribution of LO q-$\bar{q}$ subprocesses to the cross section is less than the other ones. However, by increasing the invariant mass of dilepton, its effect become larger than the other subprocesses. In panels (b), (d), and (f), the comparison between all three approaches i.e., KMR, LO-MRW and NLO-MRW are
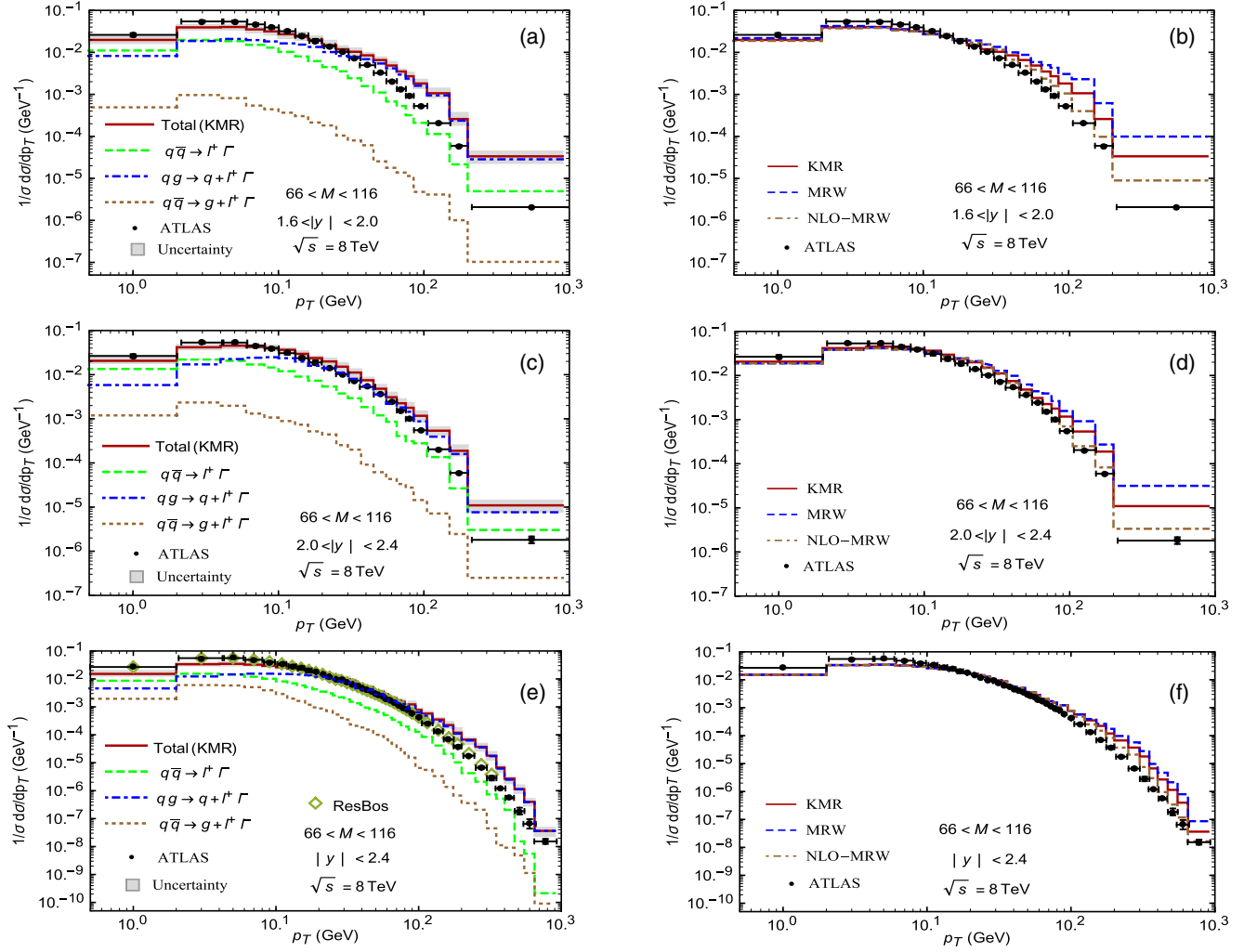
FIG. 4.   The differential cross section of Drell-Yan lepton pair production at LHC as a function of the dilepton transverse momentum at $E_{CM} = 8$ TeV compared to the ATLAS data [33]. The notation of all histograms is the same as in Fig. 1.

presented, and a similar behavior spatially at the Z boson mass region is observed. In panel (d) it is clear that the results of the three methods are more or less the same, but in panel (f) the KMR method shows better agreement with the experimental data. Our results in panels (c)–(f) are also close to those of PYTHIA [42] and SHERPA [49], especially in the small M regions, but the reggeized [54,55] model is below our predictions. According to these panels, although our results show a overestimate and underestimate in the low and high dilepton invariant mass region, the uncertainty bands of our calculations cover the experimental data. In addition, the results of the SOC and the KaTie parton-level event generator are presented in panel (f) of this figure. It is clear that there is not any significant difference between these results.

In Figs. 2–4, the normalized differential cross sections of DY as a function of p_T, at $\sqrt{s} = 7$ and 8 TeV are compared to the CMS and ATLAS Collaborations data. As expected, in all three figures, the first subprocess has the main contribution while as we go to the higher center of mass

energy i.e., 8 TeV, the second subprocess also becomes important, especially with the increase of dilepton mass [see panels (e) and (g) of the Fig. 2]. In this figure, the results of applying the SOC and the KaTie parton-level event generator are compared in panels (d) and (h), respectively. It is observed that in most of the regions, there is not a significant difference between the two methods. Also in Figs. 3 and 4 in which the rapidity is increased, only the second subprocess is sensitive to the rapidity in small p_T. However, in the large p_T region ($p_T > 10$) the contribution of second subprocess i.e., q-g, becomes enhanced and in the middle of p_T region only the first and the second subprocesses are of the same order. By considering the above three UPDF methods, one can find that for $p_T < 40$, they behave very similarly such that the LO-MRW and NLO-MRW are the upper and lower band of KMR, respectively. The experimental data also pass through the AOC band (see Ref. [56]). A comparison between our results and the parton level Monte Carlo programs such as PYTHIA and SHERPA are also presented.
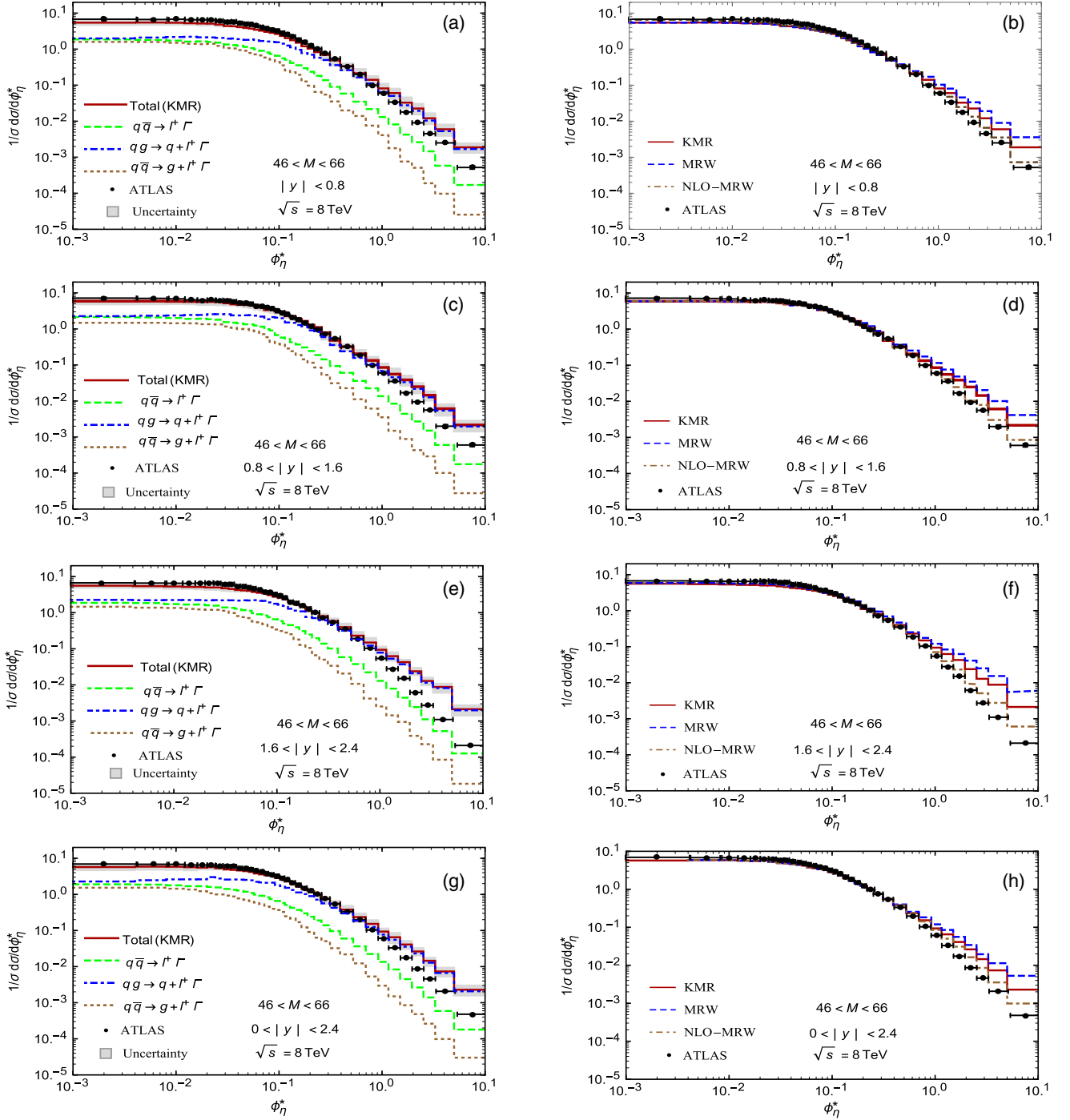
FIG. 5.   The normalized differential cross section of Drell-Yan lepton pair production at LHC as a function of ϕ_η^* at $E_{CM} = 8$ TeV compared to the ATLAS data [33]. The notation of all histograms is the same as in Fig. 1.

According to these panels, although our results show a overestimate and underestimate in the low and high dilepton invariant mass region, the uncertainty band of our calculations covers the experimental data.

In Figs. 5–8, the normalized differential cross sections of DY at LHC as a function of the variable ϕ_η^* and different experimental conditions on the dilepton rapidity and invariant mass are presented. According to these figures (except Fig. 5), it is clear that in the small ϕ_η^* region, which corresponds to the back-to-back leptons, the contribution of the first and the second subprocesses are dominated and approximately in the same order. But in Fig. 5, which is demonstrated for the small mass interval, all of the three subprocesses are of the same order for the small ϕ_η^* region. On the other hand for $\phi_\eta^* > 0.01$ the three subprocesses are separated and as it is expected contribution of the first
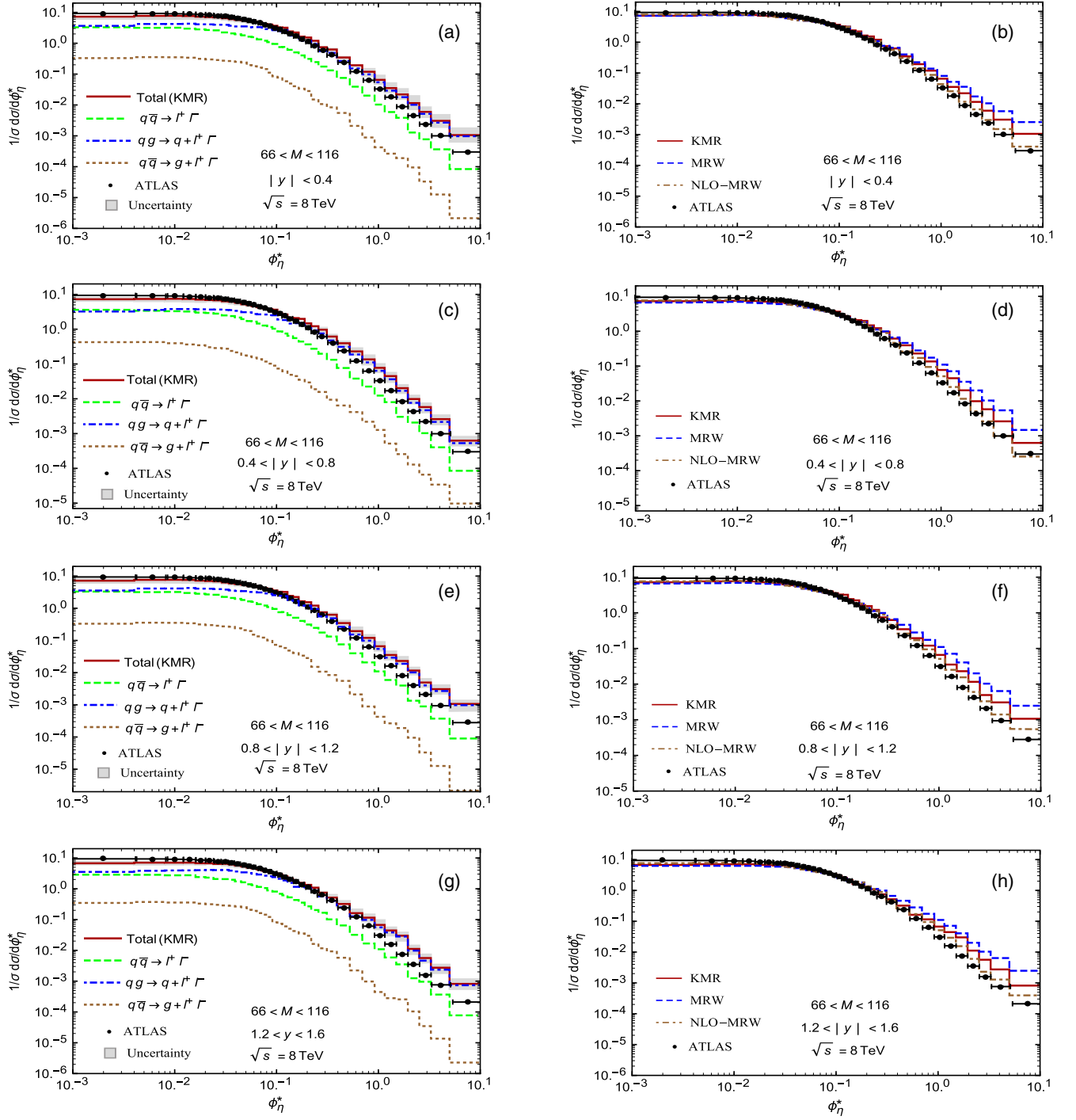
FIG. 6. The normalized differential cross-section of Drell-Yan lepton pair production at LHC as a function of ϕ_η^* at $E_{CM} = 8$ TeV compared to the ATLAS data [33]. The notation of all histograms is the same as in Fig. 1.

subprocess becomes enhanced and $\frac{d\sigma_1}{\sigma d\phi_\eta^*} > \frac{d\sigma_2}{\sigma d\phi_\eta^*} \gg \frac{d\sigma_3}{\sigma d\phi_\eta^*}$. In the right panels of these figures, the same conclusion as above can be made about the effect of different UPDF methods in which up to $\phi_\eta^* < 0.1$ they behave the same, and for larger ϕ_η the NLO-MRW UPDF cross section calculations predict closer results to the corresponding data.

The AOC and uncertainty bands approximately cover the ATLAS collaboration data.

The differential cross sections of DY with respect to the rapidity of dilepton versus y are plotted in the various panels of Figs. 9 and 10. It is observed that on average the second subprocess (qg) is dominant, especially in the mid-y region, compared to the other two subprocesses. On the
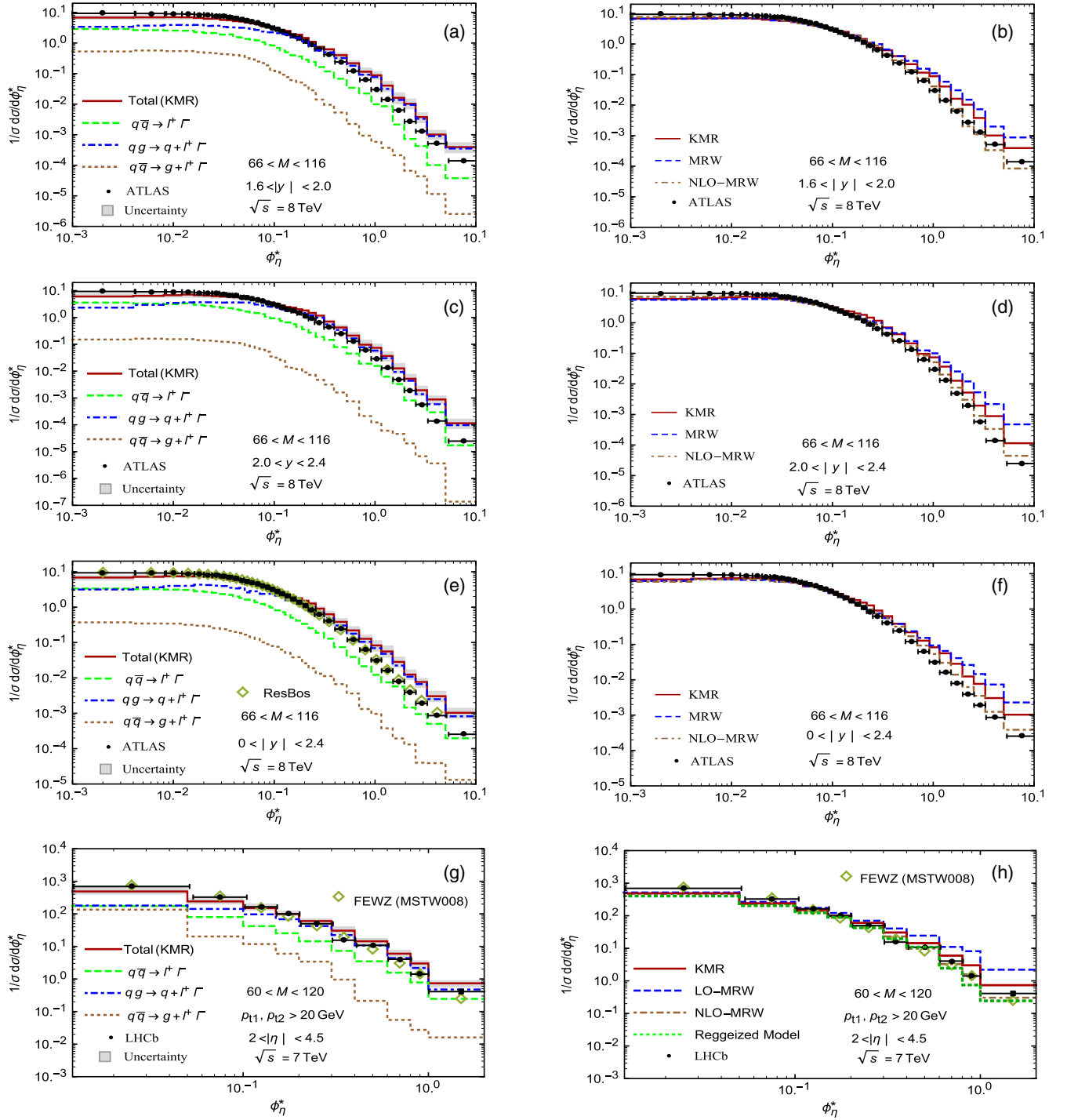
FIG. 7.   The normalized differential cross section of Drell-Yan lepton pair production at LHC as a function of ϕ_η^* at $E_{CM} = 8$ TeV compared to the ATLAS data [33]. The notation of all histograms is the same as in Fig. 1.

other hand, by comparing the right panels of these figures, one can conclude that again the NLO-MRW and KMR methods give closer results to experimental data with respect to the LO-MRW procedure.

In addition, our results are slightly different from Ref. [54] as we use different PDF, UPDF and methods. Indeed, we use the original method introduced by Kimber

et al. and consider the correct form of the normalization equation (1).

It is notable that the redefined form of normalization equation as $xa(x, \mu^2) \simeq \int^{\mu^2} dk_t^2 f(x, k_t^2, \mu^2)$ without the factor $1/k_t^2$ does not lead to the collinear form of cross section after integrating over k_t^2. In Ref. [54] the unpolarized DY in the pp collisions is investigated at the LHC
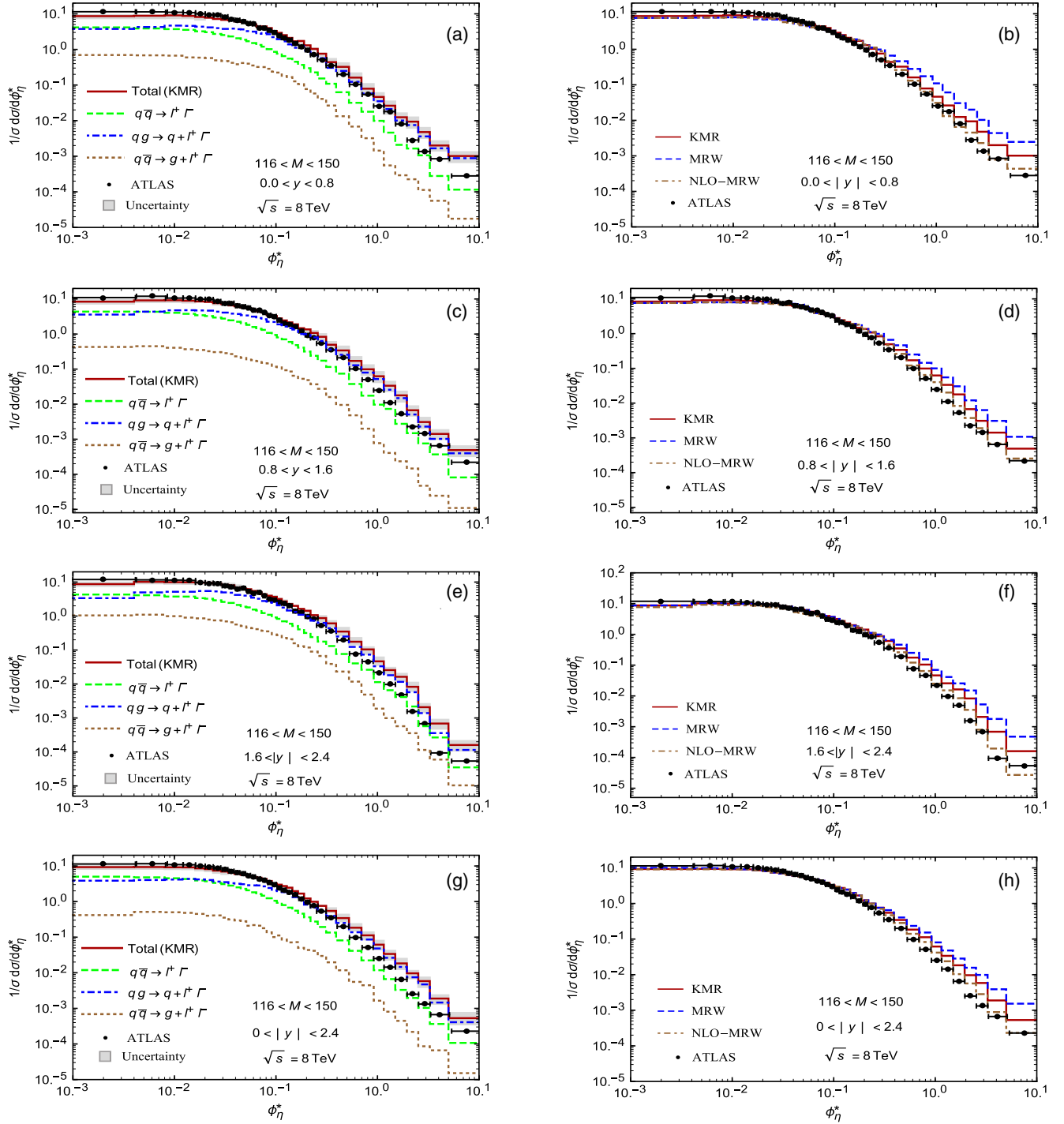
FIG. 8. The normalized differential cross section of Drell-Yan lepton pair production at LHC as a function of ϕ_η^* and dilepton transverse momentums at $E_{CM} = 8$ TeV compared to the ATLAS data [33]. The notation of all histograms is the same as in Fig. 1.

energies by CCFM and semi-KMR within the reggeized quark formalism [54,55] to be sure about the gauge invariance of matrix elements. However, as we discussed in our previous work [56], the gauge invariance is guaranteed because of applying the small x approximation in our calculations. As we pointed out before, in Figs. 1 (panel f) and 2 (panel b), our results are compared with those

of references [54,55]. On the other hand, our results are compared with those of PYTHIA [50] [Fig. 1 (panels c–f)], SHERPA [49] [Figs. 1 (panels e–f) and 3 (panels a,c,e)], FEWZ [83] [Fig. 7 (panels g–h)] and RESBOS [84] [Figs. 4 (panel e) and 7 (panel e)]. It is observed that in the regions in which the higher order calculations are not important our results are similar to those of pQCD.
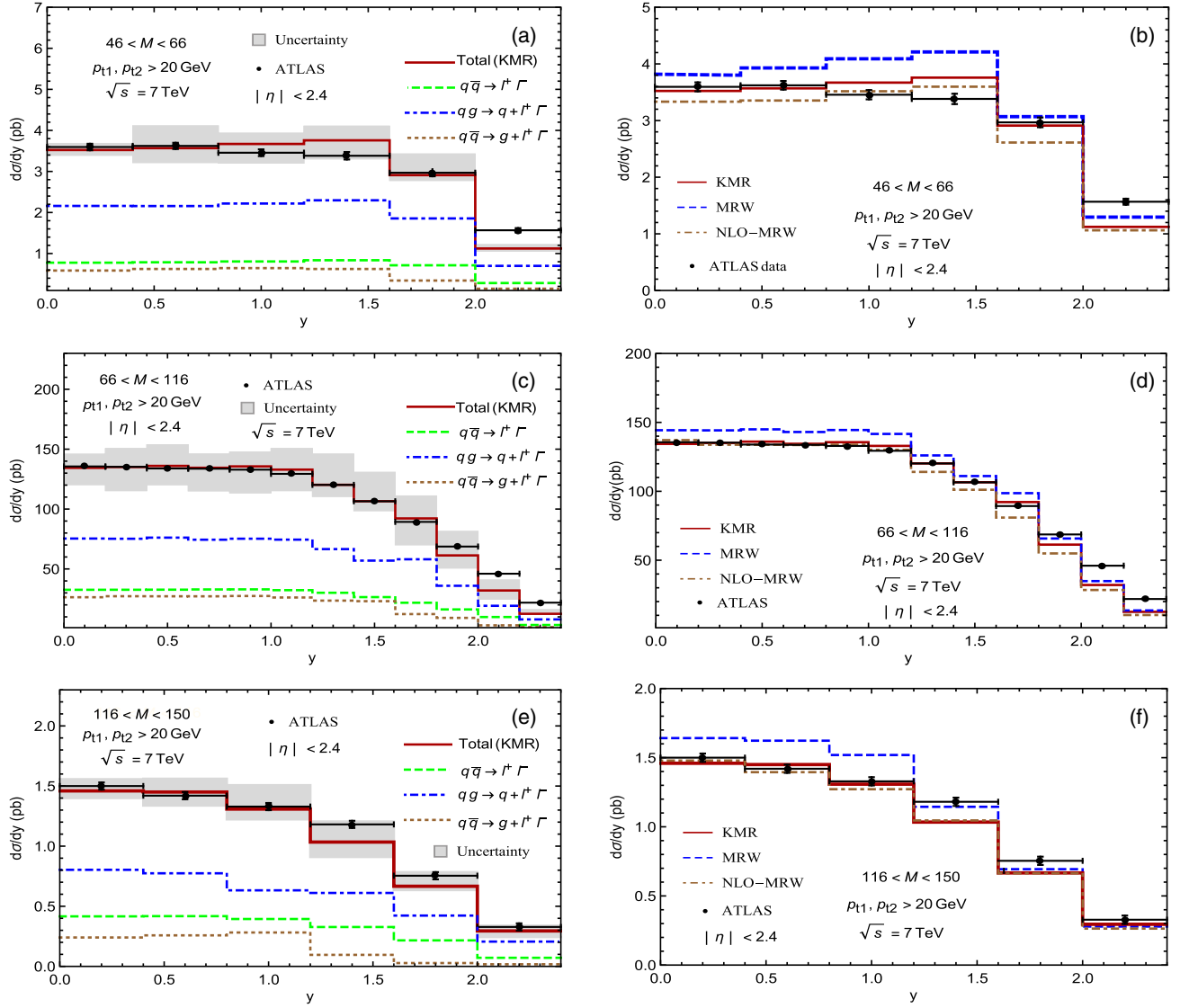
FIG. 9. The normalized differential cross section of Drell-Yan lepton pair production at LHC as a function of the dilepton rapidity at $E_{CM} = 7$ TeV compared to the ATLAS data [82]. The notation of all histograms is the same as in Fig. 1.

However, in some parts, spatially for high p_T and ϕ_η^*, the NLO-MRW UPDF scheme shows slightly different behavior with respect to the data and the pQCD methods.

In several papers such as Ref. [81], the authors denote that the description of two observables, including the p_T and ϕ_η^* distributions, are improved, if the higher order perturbative contributions are taken into account, which agrees with the cross check we performed. On the other hand as the scale of energy increases, for the LHC energies, the q-g subprocess has the largest contribution to the differential cross section in the most intervals of p_T and ϕ_η^*, as expected.

We also checked the interference effect between the γ^* and Z in the cross sections and found out that the interference is ignorable in all regions.

Finally, we would like to point out that there is a new CMS measurement on the differential cross sections of

the Z boson production in the $P - P$ collisions [85]. In Figs. 7 (in terms of p_T^Z) and 8 (in terms of ϕ_η^* of dilepton) of this report, the CMS data are compared to the theoretical works presented in Refs. [86–89], in which the UPDF [the so called transverse momentum dependent distribution functions (TMD)] are calculated, using the Parton Branching (PB) model. In this PB TMD model, the resummation to NLL accuracy, the fixed-order results at NLO, and the nonperturbative contributions are taken into account. The PB TMD results can predict the data well at low p_T^Z, but deviates from the measurements at high p_T^Z, because of missing contributions from Z + jets matrix element calculations. Furthermore, in the present work, we do not use the LHAPDF [90] or TMDlib [91] repositories, but we hope in our future papers we can analyze the difference between the applications of present
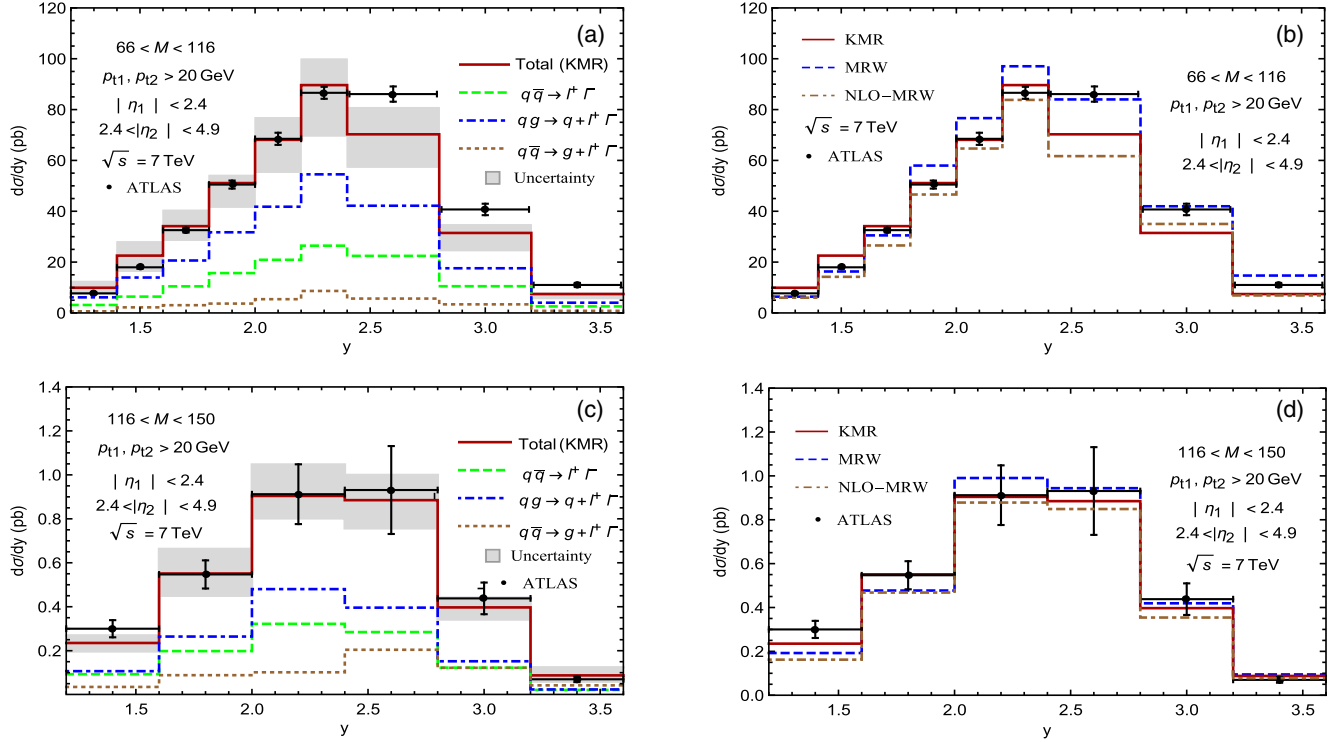
FIG. 10. The normalized differential cross section of Drell-Yan lepton pair production at LHC as a function of the dilepton rapidity at $E_{CM} = 7$ TeV compared to the ATLAS data [82]. The notation of all histograms is the same as in Fig. 1.

PDF and UPDF with those can be generated through LHAPDF and TMDlib repositories.

IV. CONCLUSIONS

We investigated the lepton pair production in the p-p and p-$\bar{p}$ collisions within the framework of k_t-factorization approach. We used the transverse momentum dependent parton distribution functions of three different prescriptions, i.e., KMR, LO-MRW and NLO-MRW. We calculated the matrix element square for the three different subprocesses among which the matrix element square for the q-$\bar{q}$ in the NLO level is rarely taken into account. We calculated several differential cross sections in terms of the dilepton invariant mass, transverse momentum and rapidity, as well as the angular correlation between produced leptons of the Drell-Yan process. In addition, we obtained the uncertainty band for the cross section distribution in the case of KMR by changing the scale factor as described in Sec. III. We considered the contribution of each subprocess separately based on the off shell and massless quarks. We found that although some of the results show that using the KMR framework, rather than LO-MRW and NLO-MRW schemes, represents better agreement with the experimental data, in the case of p_T and ϕ^*_η probing the NLO-MRW gave better predictions. It is shown that the AOC and SOC constraints give similar results and our direct calculations of the off shell matrix elements and the method of

integration for evaluation of the cross section give the same prediction as those of KaTie parton-level event generator.

Finally, in this work we consider the renormalization and factorization scales to be equal i.e., $\mu_R = \mu_F = \zeta M$, in which, M is the invariant mass of produced dilepton and ζ can vary from $1/2$ to 2, to estimate the scale uncertainties of our calculations. However as stated in Ref. [85], one can vary each scale independently. Additionally, it is possible to find the uncertainty, which comes through the implementation of PDF through UPDF, but it should not be as large as the uncertainty effect due to the variation of renormalization and factorization scales. We hope to verify these effects in our future paper.

ACKNOWLEDGMENTS

APPENDIX A: THE MATRIX ELEMENTS

The matrix elements of three subprocesses can be presented as follows:

$$\mathcal{M}_1^\gamma = ie^2 e_q \bar{v}_{s1}(k_2)\gamma^\mu u_{s2}(k_1)\frac{g_{\mu\nu}}{s}\bar{u}_{r1}(p_1)\gamma^\nu v_{r2}(p_2), \quad \text{(A1)}$$

$$M_1^Z = i \frac{g_w^2}{4\cos^2\theta_w} \bar{v}_{s1}(k_2)\gamma^\mu(C_V^q - C_A^q\gamma^5)u_{s2}(k_1) \times \left(g_{\mu\nu} - \frac{(k_1+k_2)_\mu(k_1+k_2)_\nu}{m_Z^2}\right)\frac{\bar{u}_{r1}(p_1)\gamma^\nu(C_V^e - C_A^e\gamma^5)v_{r2}(p_2)}{(s - m_Z^2 - im_Z\Gamma_Z)}, \quad \text{(A2)}$$

$$\mathcal{M}_2^\gamma = -e^2 e_q g_s t^a \varepsilon_\mu(k_2)u_{s1}(k_1)\left(\gamma^\mu\frac{\hat{k}_1+\hat{k}_2}{s}\gamma^\nu + \gamma^\nu\frac{-\hat{k}_2+\hat{p}_3}{(-k_2+p_3)^2}\gamma^\mu\right)\bar{u}_{s2}(p_3) \times \frac{g_{\mu\nu}}{(p_1+p_2)^2}\bar{u}_{r1}(p_1)\gamma^\rho v_{r2}(p_2), \quad \text{(A3)}$$

$$\mathcal{M}_2^Z = -\frac{g_w^2 g_s}{4\cos^2\theta_w} t^a \varepsilon_\mu(k_2)u_{s1}(k_1)\left(\gamma^\mu(C_V^q - C_A^q\gamma^5)\frac{\hat{k}_1+\hat{k}_2}{s}\gamma^\nu + \gamma^\nu\frac{-\hat{k}_2+\hat{p}_3}{(-k_2+p_3)^2}\gamma^\mu(C_V^q - C_A^q\gamma^5)\right)\bar{u}_{s2}(p_3)$$

$$\times \left(g_{\rho\nu} - \frac{(p_1+p_2)_\rho(p_1+p_2)_\nu}{m_Z^2}\right)\frac{\bar{u}_{r1}(p_1)\gamma^\rho(C_V^q - C_A^q\gamma^5)v_{r2}(p_2)}{(p_1+p_2)^2 - m_Z^2 - im_Z\Gamma_Z}, \quad \text{(A4)}$$

$$\mathcal{M}_3^\gamma = -e^2 e_q g_s t^a \varepsilon_\mu(p_3)u_{s1}(k_1)\left(\gamma^\mu\frac{\hat{k}_1-\hat{p}_3}{(\hat{k}_1-\hat{p}_3)^2}\gamma^\nu + \gamma^\nu\frac{-\hat{k}_2+\hat{p}_3}{(-k_2+p_3)^2}\gamma^\mu\right)\bar{v}_{s2}(k_2) \times \frac{g_{\nu\rho}}{(p_1+p_2)^2}\bar{u}_{r1}(p_1)\gamma^\rho v_{r2}(p_2), \quad \text{(A5)}$$

$$\mathcal{M}_3^Z = -\frac{g_w^2 g_s}{4\cos^2\theta_w} t^a \varepsilon_\mu(p_3)u_{s1}(k_1) \times \left(\gamma^\mu(C_V^q - C_A^q\gamma^5)\frac{\hat{k}_1-\hat{p}_3}{(\hat{k}_1-\hat{p}_3)^2}\gamma^\nu + \gamma^\nu\frac{-\hat{k}_2+\hat{p}_3}{(-k_2+p_3)^2}\gamma^\mu(C_V^q - C_A^q\gamma^5)\right)\bar{v}_{s2}(k_2)$$

$$\times \left(g_{\rho\nu} - \frac{(p_1+p_2)_\rho(p_1+p_2)_\nu}{m_Z^2}\right)\frac{\bar{u}_{r1}(p_1)\gamma^\rho(C_V^q - C_A^q\gamma^5)v_{r2}(p_2)}{(p_1+p_2)^2 - m_Z^2 - im_Z\Gamma_Z}, \quad \text{(A6)}$$

where $s = (k_1+k_2)^2$ and the electron and quark (fractional) electric charges are denoted by e and e_q. Other notations are the same as the reference [53].

APPENDIX B: THE SPLITTING FUNCTIONS

The NLO splitting functions are defined as [21]

$$\tilde{P}_{ab}^{(0+1)}(z) = \tilde{P}_{ab}^{(0)}(z) + \frac{\alpha_S}{2\pi}\tilde{P}_{ab}^{(1)}(z), \quad \text{(B1)}$$

with

$$\tilde{P}_{ab}^{(i)}(z) = P_{ab}^{(i)}(z) - \Theta(z - (1-\Delta))\delta_{ab}F_{ab}^{(i)}P_{ab}(z), \quad \text{(B2)}$$

where $i = 0$ and 1 stand for the LO and the NLO, respectively. Δ can be defined as [16]

$$\Delta = \frac{k\sqrt{1-z}}{k\sqrt{1-z} + \mu},$$

and we have

$$F_{qq}^{(0)} = C_F, \quad \text{(B3)}$$

$$F_{qq}^{(1)} = -C_F\left(T_R N_F\frac{10}{9} + C_A\left(\frac{\pi^2}{6} - \frac{67}{18}\right)\right), \quad \text{(B4)}$$

$$F_{gg}^{(0)} = 2C_A, \quad \text{(B5)}$$

$$F_{gg}^{(1)} = -2C_F\left(T_R N_F\frac{10}{9} + C_A\left(\frac{\pi^2}{6} - \frac{67}{18}\right)\right), \quad \text{(B6)}$$

$$P_{qq}(z) = \frac{(1-z^2)}{1-z}, \quad \text{(B7)}$$

$$P_{gg}(z) = \frac{z}{(1-z)} + \frac{(1-z)}{z} + z(1-z), \quad \text{(B8)}$$

[1] V. N. Gribov and L. N. Lipatov, Yad. Fiz. **15**, 781 (1972).

[2] L. N. Lipatov, Sov. J. Nucl. Phys. **20**, 94 (1975).

[3] G. Altarelli and G. Parisi, Nucl. Phys. **B126**, 298 (1977).

[4] Y. L. Dokshitzer, Sov. Phys. JETP **46**, 641 (1977).

[5] V. S. Fadin, E. A. Kuraev, and L. N. Lipatov, Phys. Lett. **60B**, 50 (1975).

[6] L. N. Lipatov, Sov. J. Nucl. Phys. **23**, 642 (1976).

[7] E. A. Kuraev, L. N. Lipatov, and V. S. Fadin, Sov. Phys. JETP **44**, 45 (1976).

[8] E. A. Kuraev, L. N. Lipatov, and V. S. Fadin, Sov. Phys. JETP **45**, 199 (1977).
[9] Ya. Ya. Balitsky and L. N. Lipatov, Sov. J. Nucl. Phys. **28**, 822 (1978).
[10] M. Ciafaloni, Nucl. Phys. **B296**, 49 (1988).
[11] S. Catani, F. Fiorani, and G. Marchesini, Phys. Lett. B **234**, 339 (1990).
[12] S. Catani, F. Fiorani, and G. Marchesini, Nucl. Phys. **B336**, 18 (1990).
[13] M. G. Marchesini, in *Proceedings of the Workshop QCD at 200 TeV Erice, Italy*, edited by L. Cifarelli and Yu. L. Dokshitzer (Plenum, New York, 1992), p. 183.
[14] G. Marchesini, Nucl. Phys. **B445**, 49 (1995).
[15] M. A. Kimber, A. D. Martin, and M. G. Ryskin, Phys. Rev. D **63**, 114027 (2001).
[16] A. D. Martin, M. G. Ryskin, and G. Watt, Eur. Phys. J. C **66**, 163 (2010).
[17] M. Modarres, H. Hosseinkhani, and N. Olanj, Nucl. Phys. **A902**, 21 (2013).
[18] M. Modarres and H. Hosseinkhani, Few-Body Syst. **47**, 237 (2010).
[19] M. Modarres and H. Hosseinkhani, Nucl. Phys. **A815**, 40 (2009).
[20] H. Hosseinkhani and M. Modarres, Phys. Lett. B **694**, 355 (2011).
[21] H. Hosseinkhani and M. Modarres, Phys. Lett. B **708**, 75 (2012).
[22] M. Modarres, H. Hosseinkhani, H. N. Olanj, and M. R. Masouminia, Eur. Phys. J. C **75**, 556 (2015).
[23] M. Modarres, M. R. Masouminia, H. Hosseinkhani, and N. Olanj, Nucl. Phys. **A945**, 168 (2016).
[24] M. Modarres, M. R. Masouminia, R. Aminzadeh Nik, H. Hosseinkhani, and N. Olanj, Phys. Rev. D **94**, 074035 (2016).
[25] M. Modarres, M. R. Masouminia, R. Aminzadeh Nik, H. Hosseinkhani, and N. Olanj, Phys. Lett. B **772**, 534 (2017).
[26] M. Modarres, M. R. Masouminia, R. Aminzadeh Nik, H. Hosseinkhani, and N. Olanj, Nucl. Phys. **B922**, 94 (2017).
[27] CMS Collaboration, J. High Energy Phys. 10 (2011) 007.
[28] CMS Collaboration, Phys. Rev. D **85**, 032002 (2012).
[29] CMS Collaboration, Phys. Lett. B **718**, 752 (2013).
[30] ATLAS Collaboration, Phys. Lett. B **705**, 415 (2011).
[31] ATLAS Collaboration, Phys. Rev. D **85**, 072004 (2012).
[32] D0 Collaboration, Phys. Rev. D **91**, 072002 (2015).
[33] ATLAS Collaboration, Eur. Phys. J. C **76**, 291 (2016).
[34] R. Aaij *et al.* (LHCb Collaboration), J. High Energy Phys. 01 (2016) 155.
[35] A. Szczurek and G. Slipek, Phys. Rev. D **78**, 114007 (2008).
[36] A. Banfi, S. Redford, M. Vesterinen, P. Waller, and T. R. Wyatt, Eur. Phys. J. C **71**, 1600 (2011).
[37] R. D. Field, *Applications of Perturbative QCD* (Addison-Wesley Publishing Company, California, 1989).
[38] R. Devenish and A. Cooper-Sarkar, Deep Inelastic Scattering (Oxford University Press, Oxford, 2004).
[39] M. Klasen, Rev. Mod. Phys. **74**, 1221 (2002).
[40] ATLAS Collaboration, Phys. Lett. B **720**, 32 (2013).
[41] A. Karlberg, E. Rea, and G. Zanderighi, J. High Energy Phys. 09 (2014) 134.
[42] CMS Collaboration, Eur. Phys. J. C **72**, 2080 (2012).

[43] L. A. Harland-Lang, A. D. Martin, P. Motylinski, and R. S. Thorne, Eur. Phys. J. C **75**, 204 (2015).
[44] K. Golec-Biernat and A. M. Stasto, Phys. Lett. B **781**, 633 (2018).
[45] N. Olanj and M. Modarres, Eur. Phys. J. C **79**, 615 (2019).
[46] B. Guiot, Phys. Rev. D **101**, 054006 (2020).
[47] B. Guiot, Phys. Rev. D **99**, 074006 (2019).
[48] G. Watt, A. D. Martin, and M. G. Ryskin, Eur. Phys. J. C **31**, 73 (2003).
[49] ATLAS Collaboration, Phys. Lett. B **725**, 223 (2013).
[50] CDF Collaboration, Phys. Rev. Lett. **87**, 131802 (2001).
[51] CDF Collaboration, Phys. Rev. D **49**, R1 (1994).
[52] F. Hautmann, L. Keersmaekers, A. Lelek, and A. M. Van Kampen, Nucl. Phys. **B949**, 114795 (2019).
[53] A. V. Lipatov, M. A. Malyshev, and N. P. Zotov, J. High Energy Phys. 12 (2011) 117.
[54] S. Baranov, A. Lipatov, and N. Zotov, Phys. Rev. D **89**, 094025 (2014).
[55] M. Nefedov, N. Nikolaev, and V. Saleev, Phys. Rev. D **87**, 014022 (2013).
[56] M. Modarres, R. Aminzadeh Nik, R. Kord Valeshabadi, H. Hosseinkhani, and N. Olanj, J. Phys. G **46**, 105005 (2019).
[57] Andreas van Hameren, Comput. Phys. Commun. **224**, 371 (2018).
[58] ATLAS Collaboration, J. High Energy Phys. 09 (2014) 145.
[59] S. Catani, M. Ciafoloni, and F. Hautmann, Nucl. Phys. **B366**, 135 (1991).
[60] M. G. Ryskin, Y. U. M. Shabelski, and A. G. Shuvaev, Phys. At. Nucl. **64**, 11 (2001).
[61] S. Baranov, A. Lipatov, and N. Zotov, Phys. Rev. D **81**, 094034 (2010).
[62] A. Lipatov and N. Zotov, Phys. Rev. D **81**, 094027 (2010).
[63] V. S. Fadin and V. E. Sherman, Pis'ma Zh. Eksp. Teor. Fiz. **23**, 599 (1976).
[64] L. N. Lipatov, Nucl. Phys. **B452**, 369 (1995).
[65] L. N. Lipatov and M. I. Vyazovsky, Nucl. Phys. **B597**, 399 (2001).
[66] A. van Hameren, P. Kotko, and K. Kutak, J. High Energy Phys. 01 (2013) 078.
[67] A. van Hameren, P. Kotko, and K. Kutak, J. High Energy Phys. 12 (2012) 029.
[68] A. van Hameren, K. Kutak, and T. Salawa, Phys. Lett. B **727**, 226 (2013).
[69] G. Marchesini and B. R. Webber, Nucl. Phys. **B310**, 461 (1988).
[70] Y. L. Dokshitzer, V. A. Khoze, S. I. Troyan, and A. H. Mueller, Rev. Mod. Phys. **60**, 373 (1988).
[71] G. Watt, Ph.D. thesis, University of Durham, United Kingdom, 2004.
[72] V. Shtabovenko, J. Phys. Conf. Ser. **762**, 012064 (2016).
[73] R. D. Field, *Application of Perturbative QCD* (Addison-Wesely Co.Inc., USA, 1989).
[74] G. P. Lepage, J. Comput. Phys. **27**, 192 (1978).
[75] M. Vesterinen and T. R. Wyatt, Nucl. Instrum. Methods Phys. Res., Sect. A **602**, 432 (2009).
[76] V. M. Abazov *et al.* (D0 Collaboration), Phys. Rev. Lett. **106**, 122001 (2011).
[77] A. Bacchetta, F. Delcarro, C. Pisano, M. Radici, and A. Signori, J. High Energy Phys. 06 (2017) 081.

[78] A. Banfi, M. Dasgupta, S. Marzani, and L. Tomlinson, Phys. Lett. B **715**, 152 (2012).

[79] R. Aaij *et al.* (LHCb Collaboration), J. High Energy Phys. 09 (2016) 136.

[80] ATLAS Collaboration, Phys. Lett. B **720**, 32 (2013).

[81] A. Gehrmann-De Ridder, T. Gehrmann, E. W. N. Glover, A. Huss, and T. A. Morgan, J. High Energy Phys. 11 (2016) 094.

[82] ATLAS Collaboration, Eur. Phys. J. C **77**, 367 (2017).

[83] LHCb Collaboration, J. High Energy Phys. 02 (2013) 106.

[84] C. Balazs, J. W. Qiu, and C. Yuan, Phys. Lett. B **355**, 548 (1995).

[85] CMS Collaboration, J. High Energy Phys. 12 (2019) 061.

[86] A. Bermudez Martinez, P. Connor, H. Jung, A. Lelek, R. Žlebčík, F. Hautmann, and V. Radescu, Phys. Rev. D **99**, 074008 (2019).

[87] F. Hautmann, H. Jung, A. Lelek, V. Radescu, and R. Zlebcik, J. High Energy Phys. 01 (2018) 070.

[88] F. Hautmann, H. Jung, A. Lelek, V. Radescu, and R. Zlebcik, Phys. Lett. B **772**, 446 (2017).

[89] A. Bermudez Martinez *et al.*, Phys. Rev. D **100**, 074027 (2019).

[90] A. Buckley, J. Ferrando, S. Lioyd, K. Nordstrom, B. Page, M. Rufenacht, M. Schonherr, and G. Watt, Eur. Phys. J. C **75**, 132 (2015).

[91] F. Hautmann, H. Jung, M. Krmer, P. J. Mulders, E. R. Nocera, T. C. Rogers, and A. Signori, Eur. Phys. J. C **74**, 3220 (2014).